Deuteron production in α-nucleus collisions from 200 to 800 MeV per nucleon

G. Montarou, J. P. Alard, J. Augerat, L. Fraysse, and M. J. Parizet
Laboratoire de Physique Corpusculaire IN2P3-CNRS, Université Blaise Pascal, F-63177 Aubière Cedex, France

R. Babinet, Z. Fodor,* J. Girard, J. Gosset, C. Laspalles, M. C. Lemaire,†
D. L'Hôte, B. Lucas, J. Poitou, W. Schimmerling,‡ and Y. Terrien
Département de Physique Nucléaire/SEPN, Centre d'Etudes Nucléaires de Saclay, F-91191 Gif-sur-Yvette Cedex, France

F. Brochard, P. Gorodetzky, and C. Racca
Centre de Recherches Nucléaires, 23 rue du Loess, B. P. 20 CR, F-67037 Strasbourg, France

J. Cugnon and J. Vandermeulen
Institut de Physique Sart Tilman, Université de Liège, B-4000 Liège 1, Belgium
(Received 27 November 1990)

Deuteron spectra at laboratory angles from 30° to 90° were measured in α+(Pb, Cu, and C) collisions at 800, 600, and 200 MeV/nucleon, and α+(Pb and C) collisions at 400 MeV/nucleon. The coalescence relation between protons and deuterons was examined for the inclusive part of the spectra. The size of the interacting region was evaluated from the observed coalescence coefficients. The rms radius is typically 4–5 fm, depending of the target mass. The proton and deuteron energy spectra corresponding to central collisions were fitted assuming emission from a single source moving with a velocity intermediate between that of the projectile and the target. The extracted "temperatures" are independent of the nature of the emitted particle, indicating that the fragments have a common source. The best fits were achieved for 200- and 400-MeV/nucleon reactions. Spectra of deuteron-like pairs, including real deuterons and neutron-proton pairs that may be contained in a larger nuclear cluster, are compared to the prediction of an intranuclear cascade model incorporating a clustering algorithm based on a classical coalescence prescription. Best agreements between experimental and predicted deuteron-like spectra occur for 800- and 600-MeV/nucleon collisions.

I. INTRODUCTION

High-energy heavy-ion collisions provide a unique tool for studying nuclear matter at excitations and densities far from the normal ground state. As the nuclei interpenetrate each other, nuclear matter is compressed and highly excited. It then expands and cools down toward lower densities and "temperatures." In the late stage of the reaction, the system disintegrates and the finally observed fragments are formed. Light composite fragments (p, d, t, ^{3}He, and ^{4}He) have been studied in relativistic heavy-ion collisions in order to study first their production mechanism [1–19] and then to extract the entropy produced in the collision [20–26]. This last aspect was particularly interesting because both hydrodynamics [27,28] and Monte Carlo calculations [15,29] predict that most of the entropy is produced in the initial phase of the collision and that this entropy, measured via the cluster abundances, may help to determine the nuclear matter equation of state. Recently, interest in light-fragment production increased since data from 200 MeV/nucleon Au+Au collisions clearly show that stronger collective effect is observed as the fragment mass increases [30,31]. The dependence of the collective effect on the mass of the emitted fragment has recently been studied in the framework of the quantum molecular dynamic model in order to determine the nuclear equation of state [32].

The production of light nuclei has been described in terms of many models: the coalescence model [1–5], taking into account the size of the deuteron and the volume of the participants [6], the quantum-mechanical sudden approximation model [7–10], thermodynamic model with chemical equilibrium [11–14], calculations using the intranuclear cascade model [15–18], and hydrodynamics coupled with thermal decay [19]. The simple coalescence model has been applied to light-particle spectra from nucleus-nucleus collisions ranging in incident energy from 20 MeV/nucleon [33–35] to 2 GeV/nucleon [3–5,36–39].

The starting point of this model is that several nucleons can fuse in a fragment with mass number A if their relative momenta are less than some coalescence radius p_0. It was shown experimentally that, at least for inclusive spectra, the cross section for a composite fragment of mass A is roughly equal to the Ath power of the observed proton cross section. However, from proton and deuteron spectra measured in a La+La collision at 800 MeV/nucleon [39], it is evident that the coalescence relation does not hold for high-multiplicity selected events. In spite of being experimentally rather successful, the simple coalescence model does not predict how p_0 depends on the fragment mass, projectile-target combina-

tions, or beam energy. Recently, a quantitative analysis [40] shows that the simplest Feynman graph corresponding to the fusion between several nucleons could serve as a theoretical basis for the coalescence model. In this model p_0 is expressed in terms of the inclusive nucleon slope parameter and the parameters which determine the short-range behavior of the deuteron wave function. The proposed approach enables the calculation of p_0 and explains its variation.

In this work we report measurements of deuteron emission in α+(Pb, Cu, and C) collisions at 800, 600, and 200 MeV/nucleon, and α+(Pb and C) collisions at 400 MeV/nucleon [41]. These results establish a link between proton- and heavy-ion-induced reactions. They were obtained with the large solid-angle detector DIOGENE at the SATURNE II synchrotron in Saclay. A brief description of the experimental setup is given in Sec. II. Double-differential cross sections are presented in Sec. III. In order to test the scaling relation predicted by the coalescence model, the deuteron spectra are compared with the second power of the observed proton spectra. From the measured scaling constant between deuteron and proton spectra, we extract the size of the interacting region. In the same section we compare the proton and deuteron production cross sections measured in the most central reactions with the predictions of a simple model assuming emission of the particles from a single source moving with a velocity intermediate between the projectile and target ones. Spectra were fitted in order to extract the "temperature" and velocity of the source.

In Sec. IV spectra of deuteron-like pairs, including real deuterons and proton-neutron pairs which may be contained in a larger nuclear cluster, are compared to the predictions of an intranuclear cascade model incorporating a clustering algorithm based on a classical coalescence prescription. The conclusions are drawn in Sec. V.

II. EXPERIMENTAL SETUP

The large solid-angle detector DIOGENE has been used at the SATURNE II synchrotron for a systematic study of α-nucleus collisions at beam energies between 200 and 800 MeV/nucleon. DIOGENE [42] is an electronic large solid-angle detector, capable of detecting and identifying the light charged fragments emitted in high-multiplicity events. For the coverage of most of the 4π sr about the beam axis, a pictorial drift chamber PDC with cylindrical symmetry surrounds the target (Fig. 1). This PDC is located in a homogeneous magnetic field parallel to the beam axis and records in three dimensions the trajectories of light charged particles in the magnetic field. Ionization electrons drift under the action of an electric field to a radial plane of multiplying wires, where the energy loss and three coordinates of each particle trajectory are sampled. A particle can be registered in the PDC if it is emitted at a polar angle θ between $\sim 15°$ and $\sim 140°$ with respect to the beam direction, and if it has enough energy to exit from the target and pass through the internal beam pipe. A barrel-shaped set of 30 plastic-scintillator slabs surrounds the PDC. In order to trigger the PDC, at least one of the 30 scintillator slabs must be fired during the reaction. A charged particle can reach one of the scintillator slabs if it has enough energy to cross the 4-mm-thick iron PDC pressure vessel in addition to the 1.5-mm stainless steel beam pipe, and if it is emitted at a polar angle between $\sim 40°$ and $\sim 120°$. DIOGENE is well suited to investigate the participant region, since this trigger provides a bias against most peripheral collisions and only fragments from the participants system lie in the PDC acceptance. The PDC and trigger acceptances for pions and baryons can be parametrized in the (y,η) plane, where y stands for the particle rapidity and η is its transverse momentum divid-

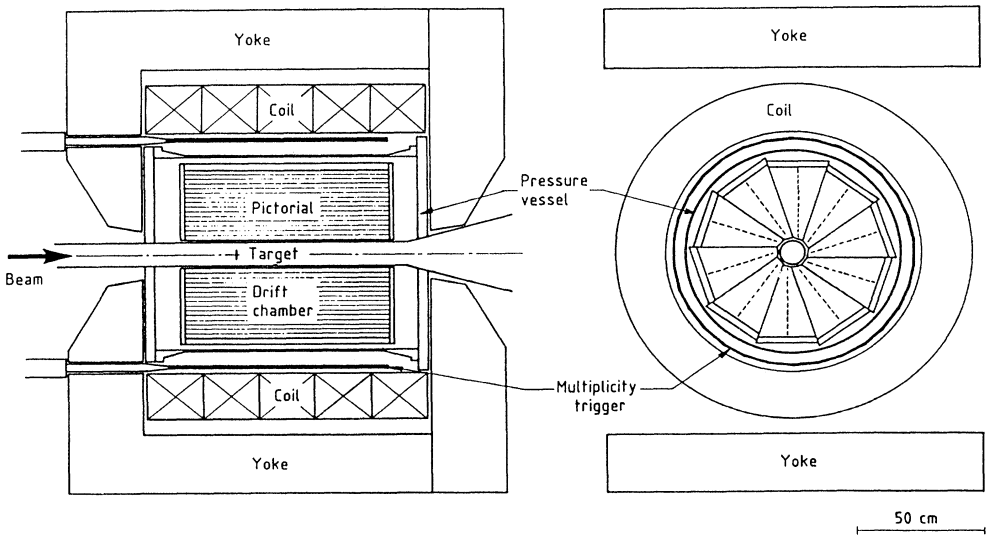

FIG. 1. Schematic views of the pictorial drift chamber of the DIOGENE facility: longitudinal (left view) and transverse (right view) sections.

ed by its mass.

All of the following analysis was made with PDC and trigger acceptances reported in Table I and displayed in Fig. 2 for protons and deuterons. The resolutions on the momentum (p) and the polar (θ) and azimuthal (ϕ) emission angles of a particle detected in the PDC result from uncertainties on the coordinates of the measured points along the track and also from multiple scattering in the target, the internal beam pipe, and the gas of the chamber. Typically, when θ becomes smaller than 30° or larger than 132°, the particles hit fewer and fewer wires, the length of the tracks inside the chamber gets smaller and smaller, and the resolutions on momentum and emission angles rapidly deteriorate. At 90° the resolutions are dominated by the target thickness. Typical values (full width at half maximum) for protons are $\Delta p/p \sim 20\%$ and of the order of few degrees for $\Delta\phi$ and $\Delta\theta$.

Charge and mass identification of each particle detected by the PDC is obtained from the correlation between energy loss and magnetic rigidity. This identification is represented in Fig. 3. The π-proton separation is excellent, and the proton-deuteron separation is good; for deuteron-triton separation, some contamination appears. This contamination arises from the experimental uncertainty on p/Z and statistical fluctuations on the energy loss in the gas of the PDC.

Raw data measured by DIOGENE consist of a large number of hits on the wires. An off-line data-analysis program deals with the track reconstruction, particle identification and computation for each reconstructed particle, of its momentum vector, and the associated uncertainties [43].

III. RESULTS

A. Double-differential cross sections

Figures 4 and 5 show the double-differential cross sections $d^2\sigma/dE\,d\Omega$ plotted versus laboratory kinetic energy of the deuteron at 30°, 50°, 70°, and 90° in the laboratory frame. We have to keep in mind that, because of the trigger conditions, only deuteron cross sections measured between 40° and 120° and above nearly 100 MeV kinetic energy are inclusive cross sections. $d^2\sigma/dE\,d\Omega$ are calculated from the deuteron production rate in intervals of ±20 MeV in kinetic energy and ±10° in polar angle. The error bars depict statistical errors only. The total systematic error on the calculated differential cross-section values is about ±15%.

TABLE I. (a) PDC acceptance for pions, protons, deuterons, and tritons, θ is the polar angle, y the rapidity, and η the transverse momentum divided by the mass. (b) Trigger acceptance for pions, protons, deuterons, and tritons.

	(a) $132° > \theta > 20°$	
	$y > 0$	$y < 0$
π	$\eta > 0.66 - 0.63y$	$\eta > 0.66 + 0.77y$
p	$\eta > 0.36 - 0.80y$	$\eta > 0.36 + 0.72y$
d	$\eta > 0.29 - 0.75y$	$\eta > 0.29 + 0.63y$
t	$\eta > 0.26 - 0.77y$	$\eta > 0.26 + 0.63y$

	(b) $120° > \theta > 40°$	
	$y > 0$	$y < 0$
π	$\eta > 0.81 - 0.33y$	$\eta > 0.81 + 0.33y$
p	$\eta > 0.41 - 0.40y$	$\eta > 0.41 + 0.30y$
d	$\eta > 0.32 - 0.53y$	$\eta > 0.32 + 0.27y$
t	$\eta > 0.28 - 0.50y$	$\eta > 0.28 + 0.40y$

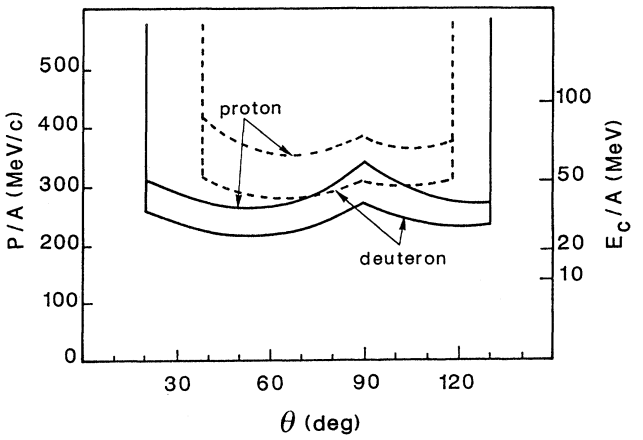

FIG. 2. Limits of PDC (solid lines) and trigger (dashed lines) acceptances for protons and deuterons as indicated in the (momentum per nucleon p/A, polar angle θ) plane. The right scale indicates the corresponding energy per nucleon.

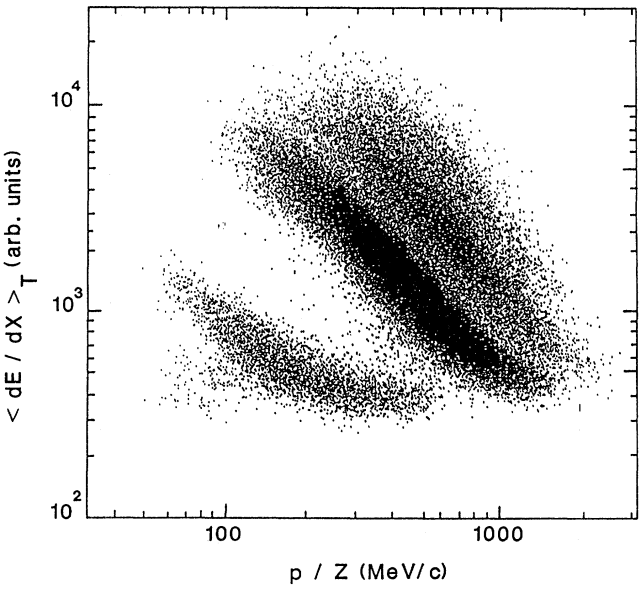

FIG. 3. $\langle dE/dX\rangle_T$ vs p/Z identification scatter plot, obtained in 800-MeV/nucleon α+Pb collisions. The mean truncated energy loss per unit length $\langle dE/dX\rangle_T$ is calculated from at least 12 samples of $\langle dE/dX\rangle$ measured along the trajectory of the particle in the PDC. The magnetic rigidity p/Z is obtained from the transverse curvature radius and the polar emission angle of the particle. From bottom left to upper right, ridges appear for pions, protons, and deuterons.

B. Coalescence model

According to the coalescence model, the invariant differential cross sections for emission of composite fragments with mass number A are related to the proton cross sections. In this model nucleons within a specified relative momentum p_0 are assumed to coalesce into light nuclei. If it is assumed that the neutron-invariant cross section is, to a first-order approximation, equal to the proton one, a simple scaling law is obtained where the composite-fragment-invariant cross section is calculated by raising the proton-invariant cross section $E_p(d^3\sigma_p/dp_p^3)$ to the power of the fragment mass number A.

The scaling relationship can be expressed as

$$E_A\left[\frac{d^3\sigma_A}{dp_A^3}\right]=C_{A/p^A}\left[E_p\left[\frac{d^3\sigma_p}{dp_p^3}\right]\right]^A, \quad (1)$$

where A is the fragment mass number, $E_A(d^3\sigma_A/dp_A^3)$ is the composite-fragment-invariant cross section at $\mathbf{p}_A$ $(=A\cdot\mathbf{p}_p)$. E_p and E_A are the proton and fragment total

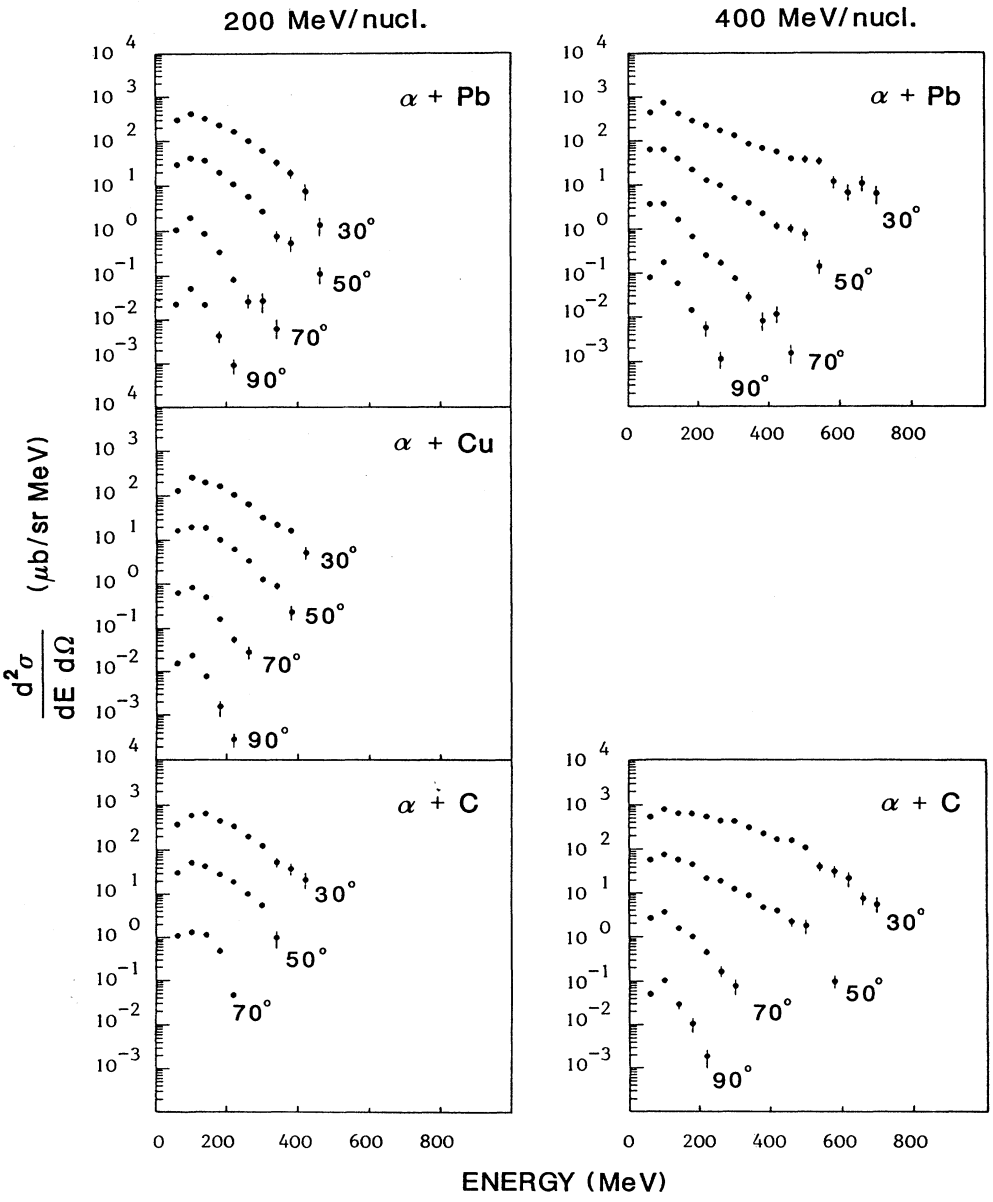

FIG. 4. Double-differential cross sections for deuterons produced in 200- (left) and 400- (right) MeV/nucleon α+Pb, Cu, or C collisions. Kinetic energy spectra at 30°, 50°, 70°, and 90° are shown for each reaction from top to bottom, multiplied by 1, 10^{-1}, and 10^{-3}, respectively. The error bars are statistical only.

energies, and C_{A/p^A} is the scaling factor. In the coalescence model this scaling factor is constant, independent of the velocity and emission angle of the fragment.

Figures 6 and 7 show the variation of the scaling factor C_{d/p^2} calculated from the observed inclusive deuteron spectra and the second power of the proton spectra measured at 50°, 70°, and 90°, as a function of the deuteron momentum. We note that the scaling law holds reasonably well; i.e., the factor C_{d/p^2} is independent of the deuteron momentum and more or less of the deuteron polar emission angle. The momentum-averaged values of the scaling factor C_{d/p^2} extracted from the observed deuteron and proton spectra measured at $\theta = 50°$, 70°, and 90° are summarized in Table II. The $\sim 15\%$ systematic error on the experimental spectra results in a $\sim 15\%$ systematic error on the scaling factor C_{d/p^2} values. In this table are also reported the momentum-averaged values of the scaling factor C_{d/p^2} extracted from Ref. [44] for the reactions $\alpha + U$ at 1050 and 400 MeV/nucleon and $\alpha + Al$ at 400 MeV/nucleon, using the same inclusive acceptance as the DIOGENE one. These data indicate a systematic variation of the scaling factor C_{d/p^2} as a function of the

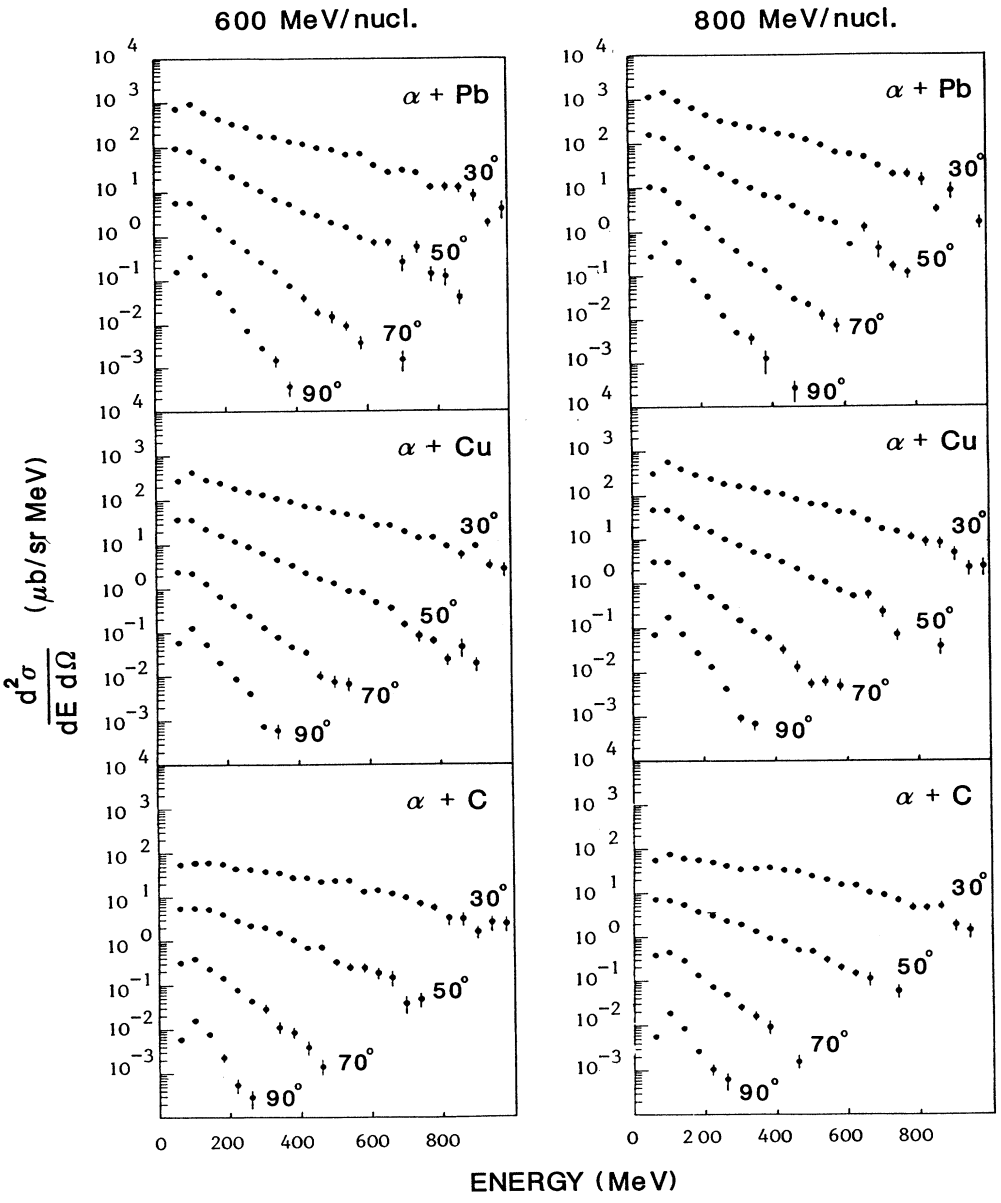

FIG. 5. Double-differential cross sections for deuterons produced in 600- (left) and 800- (right) MeV/nucleon $\alpha + Pb$, Cu, or C collisions. Kinetic energy spectra at 30°, 50°, 70°, and 90° are shown for each reaction from top to bottom, multiplied by 1, 10^{-1}, 10^{-2}, and 10^{-3}, respectively.

emission angle for the heavy target. This variation appears clearly on Fig. 8 where is represented the variation of the momentum-averaged value of the scaling factor C_{d/p^2} vs the polar emission angle in the laboratory, for the 400-MeV/nucleon α+Al and α+U reaction. One should calculate C_{d/p^2} from the primordial (preclustering) proton spectra instead of the observed one, especially when the density in phase space is large. This occurs for low momentum or forward emission and could explain the systematic variation of the scaling factor as a function of the polar emission angle for the heavy target. Nevertheless, in a first approximation one can define a mean value of the scaling factor $\langle C_{d/p^2} \rangle$ averaged over both momentum and emission angle. Figure 9 shows the beam-energy independence of this averaged scaling factor. It would imply that most of the deuterons are formed via final-state interactions in the last stage of the reaction.

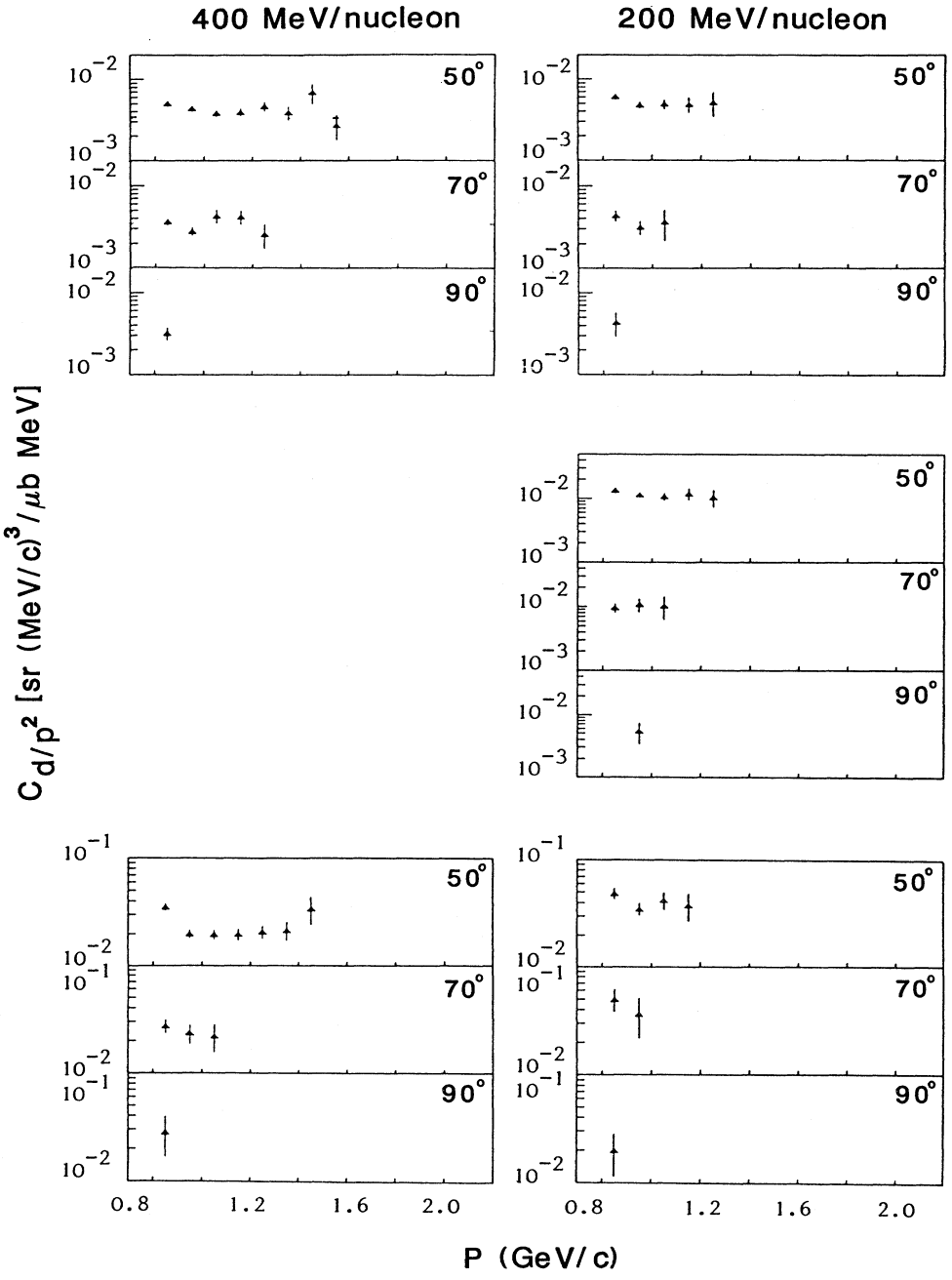

FIG. 6. Variation of the scaling factor C_{d/p^2} calculated at 50°, 70°, and 90° as a function of the deuteron momentum for α+Pb, Cu, or C (from top to bottom) collisions at 200 (right) and 400 (left) MeV/nucleon. Error bars indicate statistical error.

In the coalescence model, p_0 can be calculated from the scaling factor. In the case of deuterons, for an asymmetric target-projectile system, the expression of p_0 is [5,37]

$$p_0^3=(4m\sigma_0/\pi)\langle C_{d/p^2}\rangle[(Z_p+Z_t)/(N_p+N_t)] , \quad (2)$$

where N_p and N_t are, respectively, the projectile and target neutron numbers, Z_p and Z_t their proton numbers, m is the nucleon rest mass, and σ_0 is the geometric reaction cross section calculated from the following empirical formula [36]:

$$\sigma_0=\pi r_0^2(A_p^{1/3}+A_t^{1/3}-\delta)^2 ,$$
$$\delta=1.0-0.028A_{\min} , \quad (3)$$

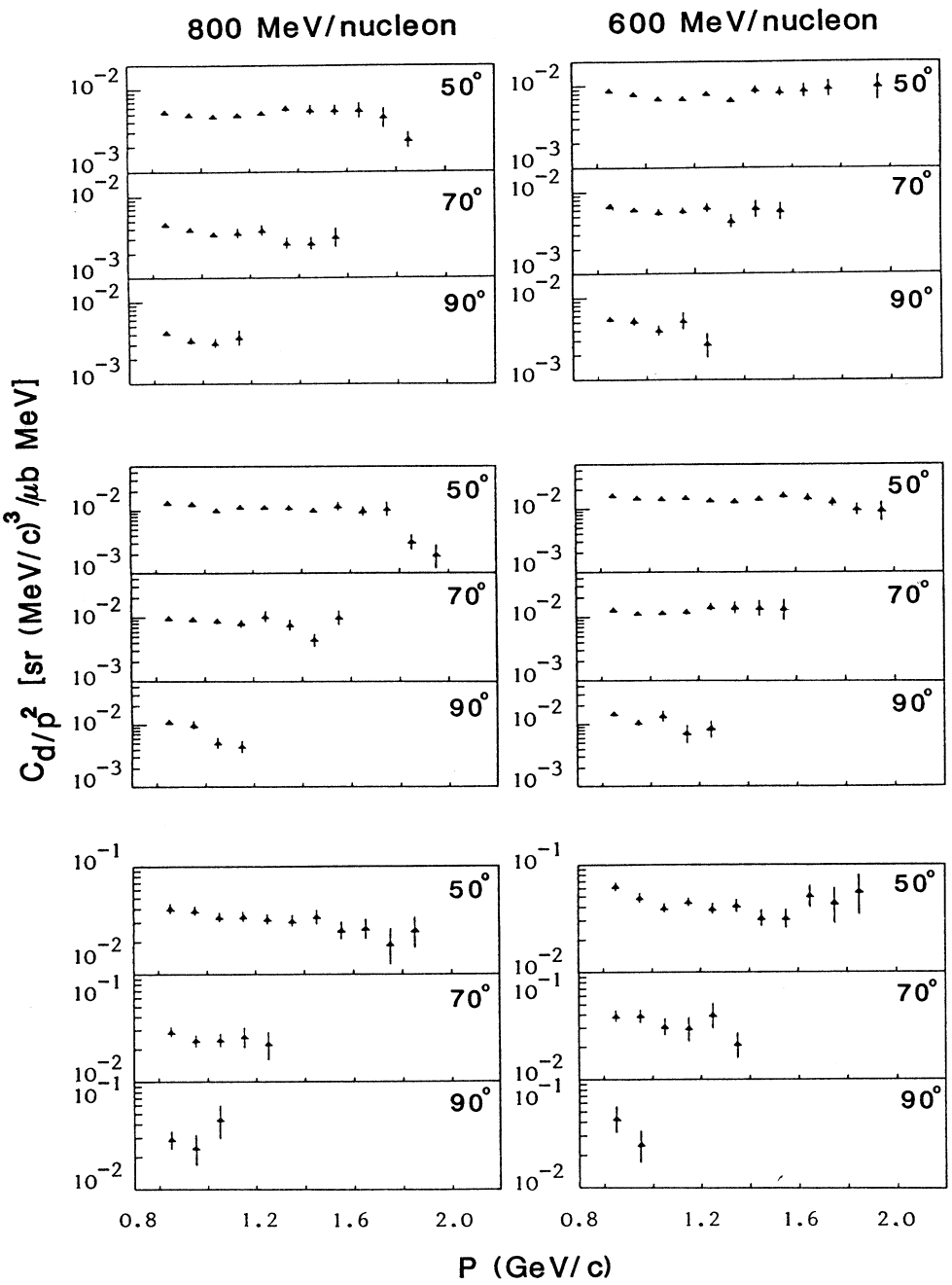

FIG. 7. Variation of the scaling factor C_{d/p^2} calculated at 50°, 70°, and 90° as a function of the deuteron momentum for α+Pb, Cu, or C (from top to bottom) collisions at 600 (right) and 800 (left) MeV/nucleon. Error bars indicate statistical error.

TABLE II. Values of the coalescence constant C_{d/p^2} [sr (MeV/c)^3/mb MeV] extracted from deuteron and proton spectra measured at laboratory angles $\theta=50°$, 70°, and 90°. $\langle C_{d/p^2}\rangle$ represents the scaling factor averaged over both momentum and emission angle. Results from α+(Pb, Cu, and C) reactions at 800, 600, 400, and 200 MeV/nucleon correspond to DIOGENE measurements. Results from α+U at 1050 and 400 MeV/nucleon, and α+Al at 400 MeV/nucleon have been calculated from Ref. [44]. Statistical errors on the measured scaling factor are indicated in parentheses.

	Energy (MeV/nucleon)	C_{d/p^2} $\theta=50°$	$\theta=70°$	$\theta=90°$	$\langle C_{d/p^2}\rangle$
Pb	800	5.0(0.6)	3.9(0.6)	3.7(0.5)	4.1(1.0)
	600	7.9(0.9)	6.2(0.6)	5.0(1.0)	6.3(1.7)
	400	4.3(0.6)	3.3(0.6)	3.2(0.6)	3.6(1.0)
	200	5.3(0.6)	3.7(0.7)	4.3(1.4)	4.5(1.3)
Cu	800	10(4.0)	8.8(1.6)	7.4(3.0)	8.7(2.3)
	600	15(1.3)	12(1.0)	12(2.8)	13(3.0)
	200	12(1.3)	10(1.3)	5.4(2.0)	10(3.2)
C	800	34(5.0)	26(3.0)	29(7.0)	28(7.0)
	600	43(8.5)	34(7.0)	32(10)	36(7.0)
	400	22(5.0)	25(3.5)	28(11)	24(6.0)
	200	41(7.0)	45(11)	20(8.2)	35(13)
Ur	1050	4.4(1.0)	3.8(0.7)	3.4(0.3)	3.7(0.6)
	400	6.0(0.9)	4.7(0.6)	4.0(0.5)	4.7(0.9)
Al	400	23(3.3)	20(2.3)	17(1.6)	19(0.5)

with $r_0=1.29$ fm, and A_p and A_t are the projectile and target atomic numbers. $A_{\min}=\min(A_p, A_t)$, and $\delta=0$ for $A_{\min}>30$.

One can relate the extracted coalescence radius to the rms radius of the interaction zone between the target and projectile nuclei, R, using the following formulation [5,37]:

$$R^3=(9h^3)/(2\pi^2 p_0^3)\ . \tag{4}$$

The rms radii of the interacting region deduced from the experimental scaling constants are plotted in Fig. 10 as a function of $(A_p^{1/3}+A_t^{1/3})$. Radii calculated in the same way from Ref. [44] for α+U and α+Al collisions are also plotted in this figure. They are quite consistent with our measurements. The relation between the extracted values of R and $(A_p^{1/3}+A_t^{1/3})$ can be approximated by a linear dependence

$$R=a(A_p^{1/3}+A_t^{1/3})+b\ , \tag{5}$$

with $a=0.30\pm0.03$ fm and $b=2.4\pm0.2$ fm.

Such a parametrization has been performed before by Nagamiya *et al.* with light-fragment measurements at laboratory angles from 10° to 145° in nuclear collisions of various projectile-target combinations, at 400, 800, and 2100 MeV/nucleon incident kinetic energies [36]. Taking into account only 800 MeV/nucleon collisions, they found rather similar values of $a=0.24\pm0.08$ fm and $b=2.0\pm0.2$ fm. The values of the rms radius R, calcu-

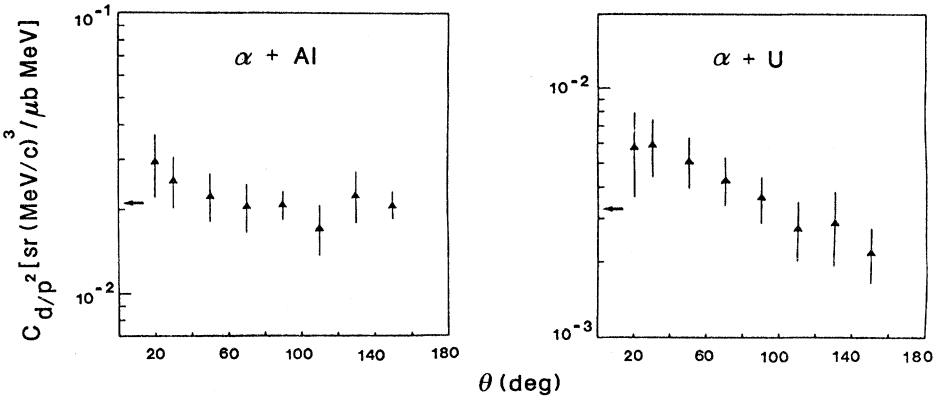

FIG. 8. Momentum-averaged scaling factor C_{d/p^2} vs the emission angle in the laboratory frame for α+Al and α+U reactions at 400 MeV/nucleon [44].

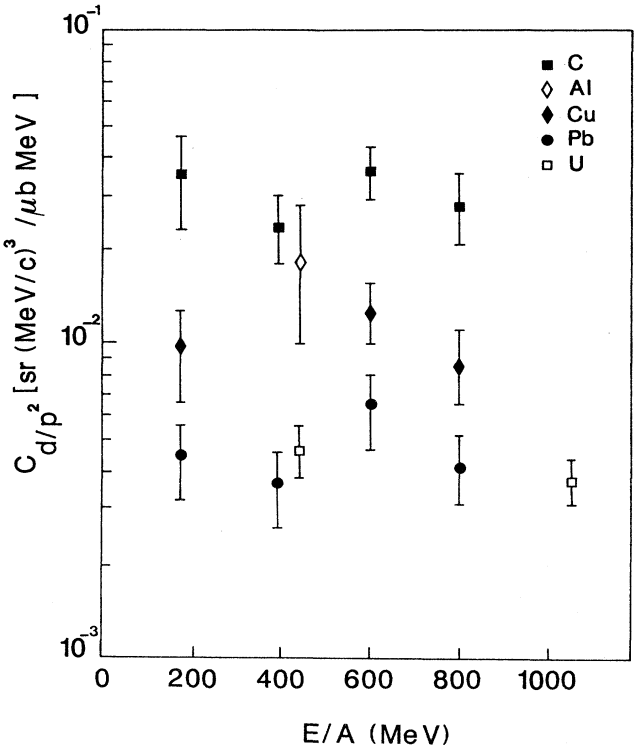

FIG. 9. Mean scaling factor $\langle C_{d/p^2} \rangle$ averaged over both momentum and emission angle versus the α incident energy per nucleon for different targets: C (solid squares), Cu (solid diamonds), and Pb (solid circles) from this experiment; Al (open diamonds) and U (open squares) from Ref. [44].

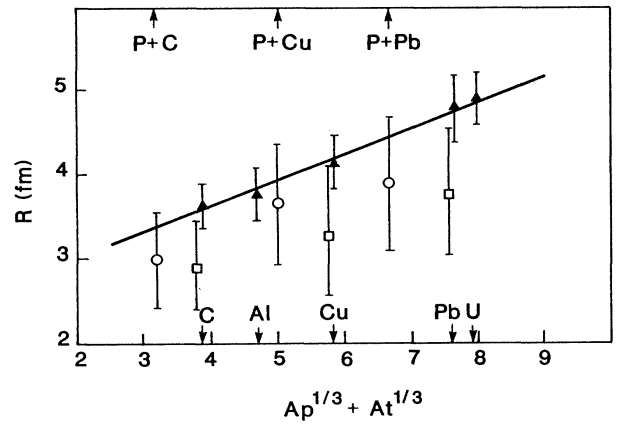

FIG. 10. Radius of the interacting region deduced from the beam-energy-averaged scaling factor vs $A_p^{1/3} + A_t^{1/3}$. Solid symbols correspond to radii evaluated from DIOGENE measurements and data from Ref. [44]. Open squares correspond to radii evaluated with the parametrization of Nagamiya *et al.* for α+Pb, Cu, or C collisions. Open circles represent radii measured in 800-MeV proton-induced collisions by Nagamiya *et al.* [36]. The solid line represents the linear dependence of the radius as expressed by Eq. (5).

lated from this parametrization, for α+C, α+Cu, and α+Pb collisions are also indicated in Fig. 10. These values are consistent with radius values given by the Eq. (5). The main difference appears for the α+Pb reaction: Equation (5) gives $R = 4.6 \pm 0.5$ fm instead of $R = 3.8 \pm 0.8$ fm calculated from the parametrization of Nagamiya *et al.* However, the experimental values of the scaling factor we used for the calculation of R are averaged over a narrow angular range ($50° \leq \theta \leq 90°$) instead of a large angular acceptance ($10° \leq \theta \leq 145°$) as in the experiment of Nagamiya *et al.* so that the determination of this averaged value is certainly affected by the detector acceptance. In Fig. 10 are also reported rms radii evaluated from proton-induced collisions with C, Cu, and Pb target nuclei measured by Nagamiya *et al.* The rms radius of the interacting zone can also be evaluated from two-particle correlations [45]. For instance two-proton correlations have been used in order to evaluate R in 3.4-GeV/nucleon p+C, d+C, and α+C collisions [46]. In the case of the α+C reaction, R has been found to lie between 3.9 and 1.7 fm, depending of the total momentum of the proton pair.

C. Parametrization of the central collisions with a single moving source

The high-energy part of the spectrum above 100 MeV kinetic energy decays approximatively exponentially with increasing energy and can be described in terms of a Maxwellian distribution observed in a moving frame. Such a distribution would occur if the particles were emitted from a thermalized gas of nucleons. We use a single source parametrization in order to characterize the emission of protons and deuterons from the participant region. This is clearly an oversimplification of the reaction mechanism, since there are certainly a continuum of sources for intermediate-rapidity fragments. However, we use this parametrization to compare various sets of data and explore the evidence for thermalization. The distribution is assumed to be isotropic in a frame moving with the velocity β (relative to the speed of light) in the laboratory frame. The laboratory spectra of particles emitted from the source are obtained by transforming relativistically from the source rest frame to the laboratory:

$$\frac{E}{p^2}\frac{d^2\sigma}{dp\,d\Omega} = C\gamma(E - \beta p\cos\theta)\exp\left[-\frac{\gamma(E-\beta p\cos\theta)}{T}\right], \tag{6}$$

where $E = (p^2 + m^2)^{1/2}$ and $\gamma = 1/(1-\beta^2)^{1/2}$. C is a constant, and m is the mass of the particle (proton or deuteron) emitted at angle θ with momentum p. The parameters C, T, and β are determined by using a least-squares method to fit the invariant differential cross sections. The thermodynamic language has regained popularity in the field of high-energy heavy-ion collisions, and it has become a habit to call the slope parameter T the "temperature" of the moving source. This practice neglects all the problems and hidden assumptions connected with the measurement of the "temperatures" reached in heavy-ion reactions, but it has the advantage of summar-

izing the spectra in an easy way and allowing systematic analysis as a function of incident energy and target/projectile ion mass number.

In order to isolate the component of the spectra originating from the participant source, a selection criterion was established. It is evident that the spectra measured at polar emission angles $\theta \geq 50°$ and kinetic energy greater than 100 MeV consist of particles emitted by this participant source, and so the parameters are determined by using only that part of the measured spectra. In addition, an impact parameter selection is performed using the total nuclear charge multiplicity $M_{\tilde{p}}$ measured in the PDC acceptance and defined by

$$M_{\tilde{p}} = M_p + M_d + M_t \ , \tag{7}$$

where M_p, M_d, and M_t are the proton, deuteron, and triton multiplicities measured in the proton acceptance as defined in Table I(a). This selection is based on the strong correlation between the centrality of the collision and the multiplicity $M_{\tilde{p}}$: The more the collision is central, the more $M_{\tilde{p}}$ increases. For convenience, this selection is presented as a function of the squared reduced impact parameter $\tilde{b}^2 = b^2/(R_p + R_t)^2$, where b stands for the impact parameter, and R_p and R_t are the radii of the projectile and target nuclei, respectively. The quantity $\tilde{b}^2$ is estimated from the $M_{\tilde{p}}$ distribution as the ratio of the integrated cross section to the geometrical one [Eq. (3)], with the integration starting from the highest multiplicity bin, and assuming a one-to-one correspondence between

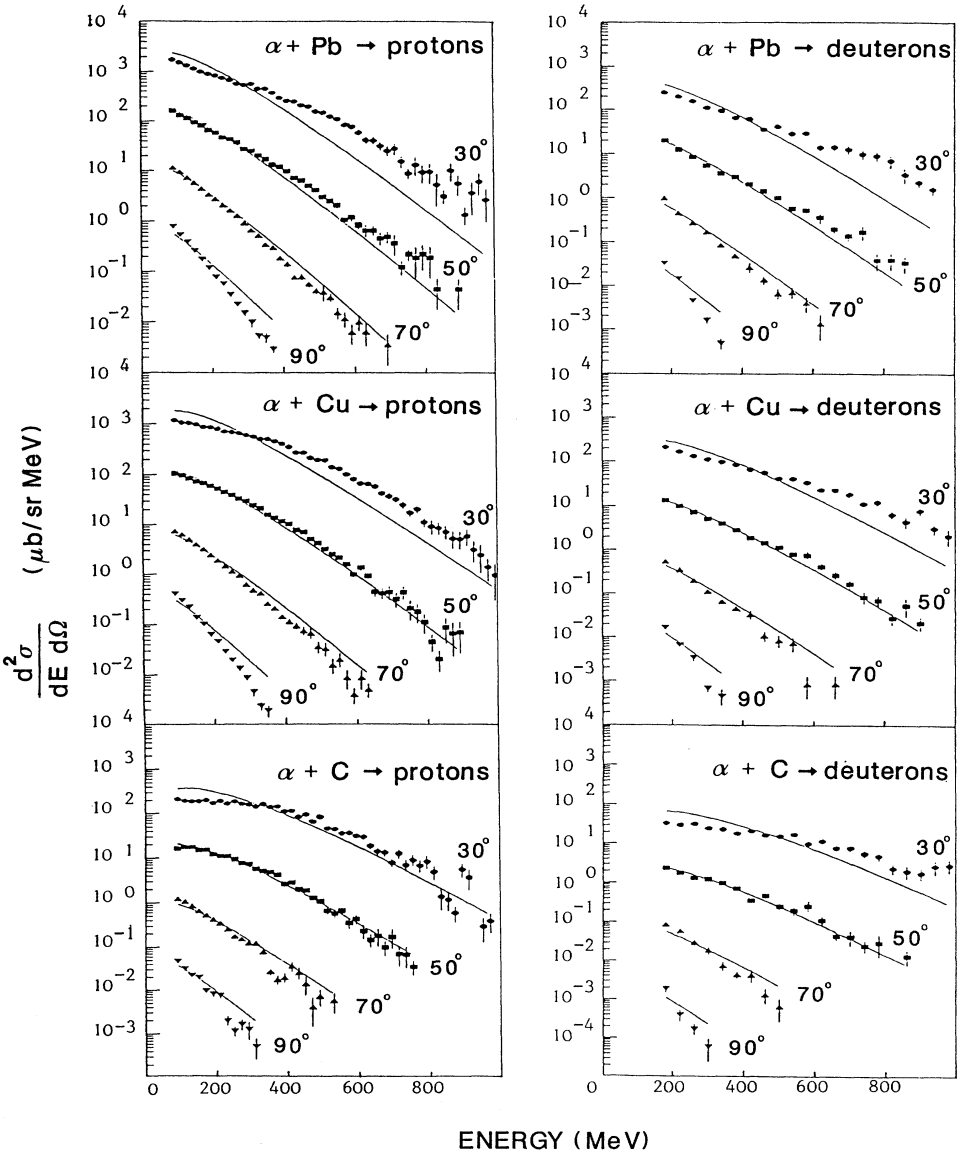

FIG. 11. Double-differential cross sections for protons (left) and deuterons (right) produced in the most central collisions of α with Pb (top), Cu (middle), and C (bottom) at 800 MeV/nucleon. Kinetic energy spectra at 30°, 50°, 70°, and 90° are shown for each reaction from top to bottom, multiplied by 1, 10^{-1}, 10^{-2}, and 10^{-3}, respectively. The solid lines indicate the results of the single-moving-source parametrization.

increasing impact parameter and decreasing multiplicity [47].

Proton and deuteron double-differential cross sections measured in the most central collisions are compared in Figs. 11–14 to the results of this analysis. The best fits are achieved at low bombarding energies (400 and 200 MeV/nucleon). For high bombarding energies (800 and 600 MeV/nucleon), the 30° spectra are systematically underestimated by the fitting procedure in the region it considers, i.e., the high-energy tail of the distribution. It can result from the fact that these spectra include substantial contribution from light particles emitted with rapidity near the projectile rapidity. The other important apparent feature of Figs. 11 and 12 is that the single source emission is not able to reproduce the variation of the slope of the 800- and 600-MeV/nucleon spectra as a function of the emission angle. It suggests that light particles produced in 800- and 600-MeV/nucleon reactions do not originate from a single thermalized moving source.

The "temperatures" and source velocities extracted from proton and deuteron spectra are reported in Table III. For each reaction we give the minimum value of the multiplicity M_p used in order to select central events and the mean value of the squared reduced impact parameter $\langle \tilde{b}^2 \rangle$ corresponding to this selection. Parameters deduced from proton and deuteron spectra are quite similar. We can analyze the parameters extracted from the 200- and 400-MeV/nucleon reactions with a simple mod-

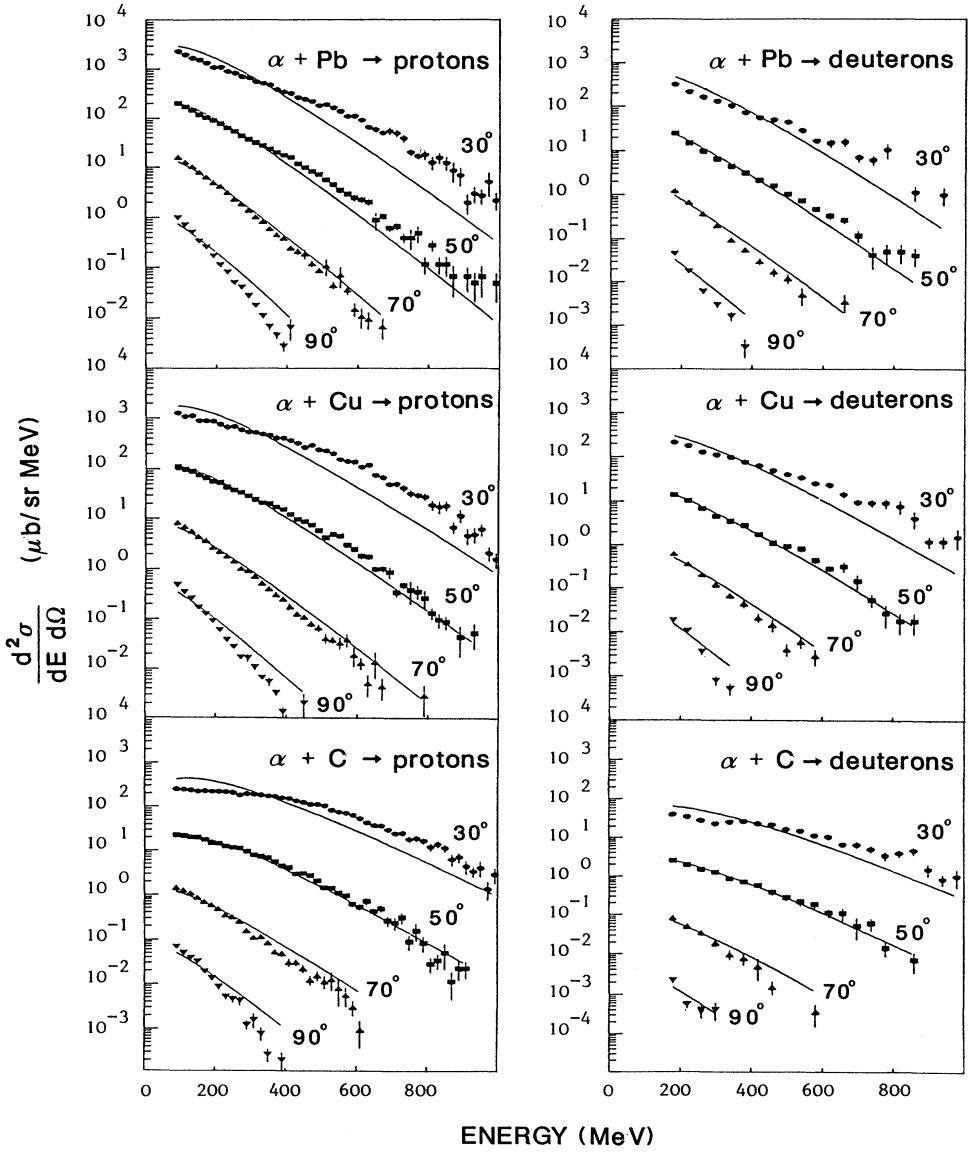

FIG. 12. Double-differential cross sections for protons (left) and deuterons (right) produced in the most central collisions of α with Pb (top), Cu (middle), and C (bottom) at 600 MeV/nucleon. Kinetic energy spectra at 30°, 50°, 70°, and 90° are shown for each reaction from top to bottom, multiplied by 1, 10^{-1}, 10^{-2}, and 10^{-3}, respectively. The solid lines indicate the results of the single-moving-source parametrization.

el using the basic concepts of the fireball model [4]. If one assumes that the source velocity in the laboratory (β_S) depends only on the relative number of participant nucleons coming from the projectile and target, β_S can be expressed as a function of $x = n_p/(n_p+n_t)$, where n_p and n_t are the number of participant nucleons from the projectile and target, respectively:

$$\beta_S = \frac{n_p[t(t+2m')]^{1/2}}{(n_p+n_t)m'+n_p t} = \frac{x[t(t+2m')]^{1/2}}{m'+xt} , \quad (8)$$

where t is the projectile incident kinetic energy per nucleon and m' is the mass of a bound nucleon (taken to be 931 MeV). The total energy per nucleon in the center of mass of the source is given by

$$e_{\text{c.m.}} = m'[1+2x(1-x)t/m']^{1/2} . \quad (9)$$

Moreover, the source can be treated as a nonrelativistic equilibrated ideal gas where all the available kinetic energy of the participant nucleons is completely randomized. Consequently, the source "temperature" is given by

$$\tfrac{3}{2}T_S = (e_{\text{c.m}} - m) , \quad (10)$$

where m is the mass of a free nucleon. For α+Pb 400-MeV/nucleon collisions, the experimental source velocity β_S equal to 0.25 (relative to the speed of light) corresponds to $x=0.27$ in Eq. (8). Putting this value in Eqs. (9) and (10) gives a source "temperature" T_S equal to 42 MeV, in comparison with the extracted proton "temperature" $T_p=43$ MeV. Assuming, for such a central reaction ($\langle \tilde{b}^2 \rangle \sim 0.114$), that the number of participant nucleons from the α projectile (n_p) is equal to 4, one calculates, from the definition of x, the corresponding value of n_t. For α+Pb 400-MeV/nucleon collisions, one thus obtains $n_t=11$. This value can be compared with the number of nucleons $n_{\text{c.c.}}$, which are contained in the target nucleus volume delimited by clean cylindrical cuts of the target sphere by the projectile. For the collision of two uniform density spheres, representing α and Pb nuclei with a mean-square-reduced impact parameter $\langle \tilde{b}^2 \rangle = 0.114$, $n_{\text{c.c.}}$ is found equal to ~ 19. However, the clean-cut definition of the geometrical interaction volume is based on the assumption that the accumulated scattering angle of the incident projectile nucleons is small; i.e., a given projectile nucleon interacts only with those target nucleons which are located in a narrow tube along its straight trajectory. As a matter of fact, this particular simplification is certainly not completely justified for a low-incident-energy reaction. The results extracted from 200- and 400-MeV/nucleon α+Pb, Cu, or C reactions are reported in Table IV.

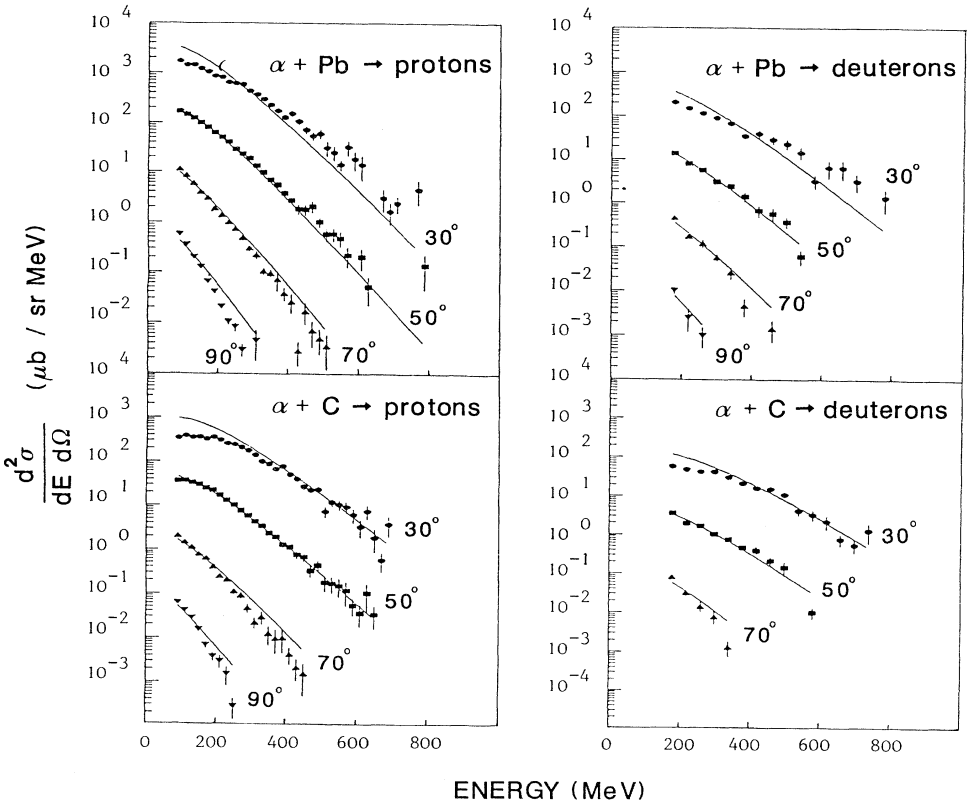

FIG. 13. Double-differential cross sections for protons (left) and deuterons (right) produced in the most central collisions of α with Pb (top), Cu (middle), and C (bottom) at 400 MeV/nucleon. Kinetic energy spectra at 30°, 50°, 70°, and 90° are shown for each reaction from top to bottom, multiplied by 1, 10^{-1}, 10^{-2}, and 10^{-3}, respectively. The solid lines indicate the results of the single-moving-source parametrization.

IV. EXTENSION OF THE INTRANUCLEAR CASCADE FOR THE CALCULATION OF THE DEUTERON-LIKE CROSS SECTIONS

A. Description of the model

We now describe briefly the extension of the intranuclear cascade model used in this paper for the comparison with our data. In this model the collision of the two nuclei is described by straight-line propagation of nucleons between scattering points. We have used the Cugnon cascade code [48,49]. In that code binary collisions between nucleons and Δ resonances are computed, and the Δ's have a finite lifetime. The isospin of each particle is explicitly incorporated. The original code is improved by "freezing" the spectators until they interact [50]. The impact parameter of the intranuclear-cascade-simulated events spreads over 10 b values from 0 to $9(R_p+R_t)/9.5$. For each impact parameter, we compute, respectively, 1000, 1500, and 3000 events for α+Pb, Cu, and C reaction.

As the intranuclear cascade follows the A-body phase-space coordinates of all the nucleons, composite-fragment production can be calculated via a clustering algorithm based on a generalized coalescence formula involving both momentum and spatial coordinates [18]. The prob-

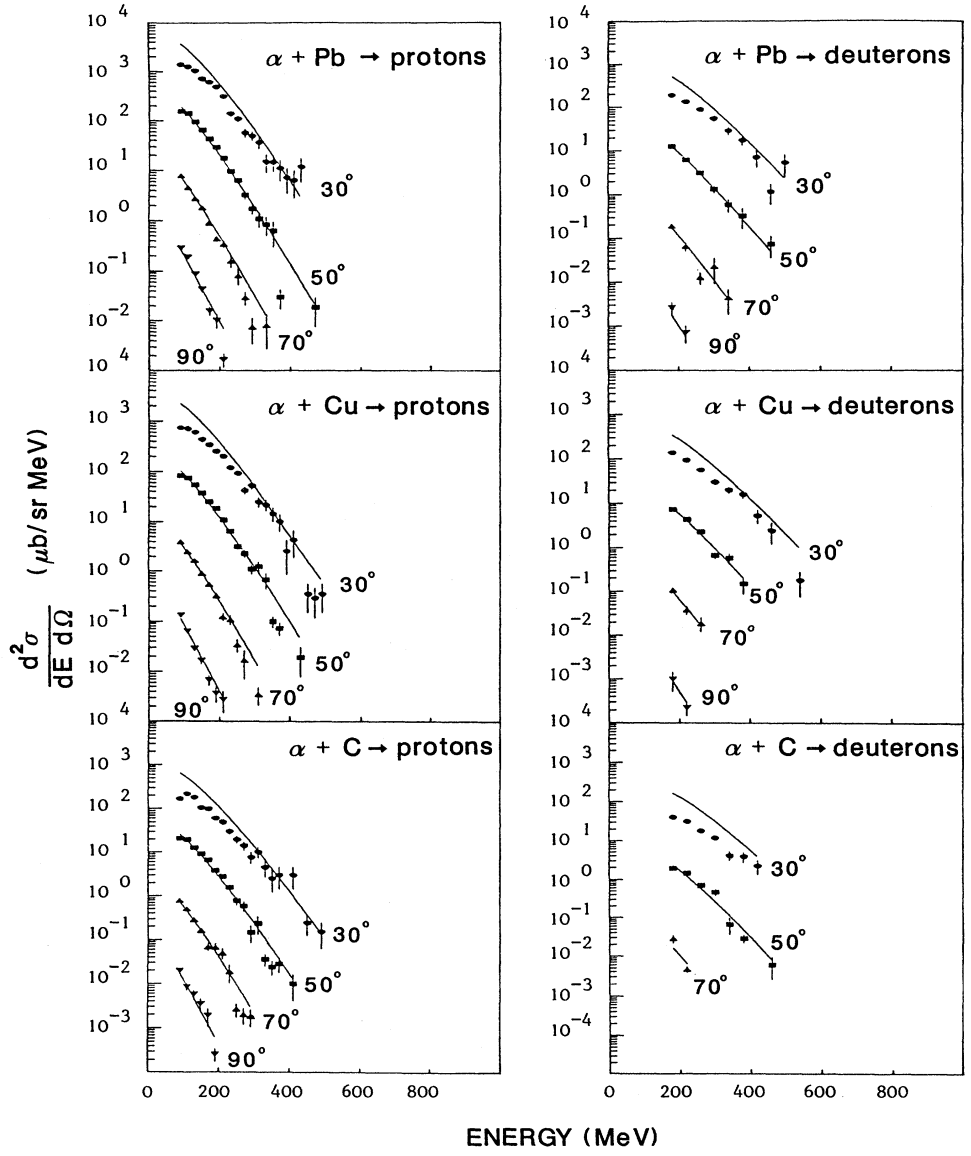

FIG. 14. Double-differential cross sections for protons (left) and deuterons (right) produced in the most central collisions of α with Pb (top), Cu (middle), and C (bottom) at 200 MeV/nucleon. Kinetic energy spectra at 30°, 50°, 70°, and 90° are shown for each reaction from top to bottom, multiplied by 1, 10^{-1}, 10^{-2}, and 10^{-3}, respectively. The solid lines indicate the results of the single-moving-source parametrization.

TABLE III. Slope parameters (T) and source velocities (β) determined by a least-squares fit to the high-energy tails ($E \geq 100$ MeV/nucleon) of the spectra measured at polar emission angles $>= 50°$. The most central collisions are selected by requiring that the charged baryon multiplicity be greater than $M_{\tilde{p}}$. $\langle \tilde{b}^2 \rangle$ is the average squared reduced impact parameter for these central collisions. T_p and β_p refer to parameters determined using proton spectra, and T_d and β_d correspond to deuteron spectra. Errors on the fitted parameters are indicated in parentheses.

	Energy (MeV/nucleon)	$M_{\tilde{p}}$	$\langle \tilde{b}^2 \rangle$	T_p (MeV)	β_p	T_d (MeV)	β_d
Pb	800	4	0.123	60(3)	0.24(0.09)	59(3)	0.22(0.08)
	600	3	0.104	57(3)	0.24(0.05)	59(3)	0.23(0.06)
	400	2	0.114	43(3)	0.25(0.04)	46(3)	0.25(0.03)
	200	1	0.100	29(1)	0.22(0.02)	31(2)	0.25(0.02)
Cu	800	3	0.138	64(4)	0.30(0.08)	62(4)	0.26(0.06)
	600	2	0.154	59(3)	0.30(0.06)	64(4)	0.28(0.06)
	200	1	0.09	29(3)	0.24(0.02)	32(1)	0.26(0.02)
C	800	2	0.100	66(7)	0.39(0.05)	67(4)	0.34(0.03)
	600	2	0.08	60(4)	0.38(0.04)	63(4)	0.35(0.05)
	400	1	0.134	43(2)	0.35(0.02)	47(6)	0.32(0.03)
	200	1	0.05	27(2)	0.27(0.02)	28(1)	0.30(0.02)

ability for each different n-p pair to form a deuteron is determined by their relative separation and momentum when both cease to interact with other nucleons of the system. For two nucleons labeled i,j, let us denote by t_{ij} the last interaction time of either of them with any other nucleon (t_{ij} can vary over the entire history of the reaction), by $\mathbf{x}$ and $\mathbf{p}$ their position and momentum. Thus their relative momentum $\mathbf{q}(t_{ij})$, relative position $\mathbf{r}(t_{ij})$, and the total momentum $\mathbf{P}(t_{ij})$ at time t_{ij} is written as

$$\begin{aligned} \mathbf{q}(t_{ij}) &= [\mathbf{p}_i(t_{ij}) - \mathbf{p}_j(t_{ij})]/2 \ , \\ \mathbf{r}(t_{ij}) &= \mathbf{x}_i(t_{ij}) - \mathbf{x}_j(t_{ij}) \ , \\ \mathbf{P}(t_{ij}) &= \mathbf{p}_i(t_{ij}) + \mathbf{p}_j(t_{ij}) \ . \end{aligned} \tag{11}$$

From the relative position $\mathbf{r}(t_{ij})$ and the relative momentum $\mathbf{q}(t_{ij})$ of the n-p pair, one evaluates the following function where d_1 is a constant and $\hbar$ is taken equal to 1:

$$F(\mathbf{r}(t_{ij}),\mathbf{q}(t_{ij})) = \exp[-r^2(t_{ij})/d_1^2 - q^2(t_{ij})d_1^2] \ . \tag{12}$$

Then the coalescence condition is expressed as

$$F(\mathbf{r}(t_{ij}),\mathbf{q}(t_{ij})) \leq d_2 \ , \tag{13}$$

where d_2 is a dimensionless constant. It was found that the best agreement between the intranuclear cascade predictions and experimental data occurs for $d_1 = 1.7$ fm and $d_2 = 0.04$. In fact, with the coalescence procedure, we can only calculate primordial deuteron (deuteron-like) and primordial proton (proton-like) cross sections. Experimental deuteron-like and proton-like cross sections are related to the experimental light-particle cross sections for composites by the usual expressions [15]:

$$\begin{aligned} \sigma_{\mathrm{DL}} &= \sigma_d + 1.5\sigma_t \ , \\ \sigma_{\mathrm{PL}} &= \sigma_p + \sigma_d + \sigma_t \ . \end{aligned} \tag{14}$$

Since the triton contribution is weighted by a factor of $\frac{3}{2}$, the experimental deuteron-like multiplicity can take noninteger values.

Nucleons before and during the reaction find themselves in an average optical potential. They must overcome this potential to energy unbound of the system. This effect is not included in the code. Therefore, in order to correct for it, we introduced a momentum-shift correction to the direct output of the cascade code. Each final nucleon momentum $p_i(t_{ij})$ is transformed into [18]

TABLE IV. Calculated properties of the source in α+Pb, Cu, or C 200- and 400-MeV/nucleon collision with mean-square-reduced impact parameter $\langle \tilde{b}^2 \rangle$. The relation between the source velocity β_S and x is given by Eq. (8). The corresponding source "temperature" T_S is estimated from Eqs. (9) and (10), and can be compared to the measured proton "temperature" T_p. $\langle n_t \rangle$ is the mean number of participant nucleons from the target, assuming that n_p is equal to 4 in Eq. (8). This value can be compared with the number of nucleons $n_{\mathrm{c.c.}}$, which are contained in the target nucleus volume delimited by clean cylindrical cuts of the target uniform density sphere by the projectile.

	Energy (MeV/nucleon)	$\langle \tilde{b}^2 \rangle$	β_S	x	T_S (MeV)	T_p (MeV)	$\langle n_t \rangle$	$n_{\mathrm{c.c.}}$
Pb	400	0.114	0.25	0.27	42	43(3)	11	19
	200	0.100	0.22	0.34	25	29(1)	8	20
Cu	200	0.09	0.24	0.38	26	29(3)	7	13
C	400	0.134	0.35	0.40	56	43(2)	6	5
	200	0.05	0.27	0.43	27	27(2)	5	7

$$p_i'(t_{ij})=[p_i(t_{ij})^2+2mV_0]^{1/2}\ , \qquad (15)$$

where V_0 was fixed in order to reproduce the proton-like and deuteron-like total production cross sections. A best value of $V_0 \sim -39$ MeV was found.

In comparing theoretical predictions of the intranuclear cascade and the experimental data, we have to take into account the distortion induced by the inefficiencies of the detector. The main biases of the PDC are the experimental cuts on angle and energy. Through the intranuclear cascade code and coalescence prescription, we can only calculate primordial proton and deuteron distributions. It is then necessary to reduce the PDC acceptance to the proton one for proton-like distributions and to the deuteron one for deuteron-like distributions. Moreover, in order to trigger the PDC, at least one of the 30 plastic-scintillator slabs surrounding the PDC must be fired during the reaction. In order to eliminate events triggered by a neutral particle in the barrel of scintillators, we apply the software condition in the analysis that an event is accepted only if, among the charged particles detected in the PDC, there is a pion or a proton-like particle which can reach one of the scintillator slabs. As for the PDC acceptance, we reduce the proton-like trigger acceptance to the proton one.

B. Results

The proton-like and deuteron-like total cross-section measurements in DIOGENE are displayed in Fig. 15, where the experimental results are compared to the cascade predictions. The energy variation of the total cross section is roughly reproduced by the cascade predictions (experimental results are affected with a $\sim 15\%$ systematic error). For $\alpha+$Cu and $\alpha+$Pb collisions, the cascade predictions are larger than the experimental results. This appears in Fig. 15, where are also displayed the mean proton-like and deuteron-like multiplicities measured per event. These figures show that this disagreement increases with the incident energy. Such a discrepancy has also been observed for proton-like multiplicity distributions [51]. It is obvious that the momentum-shift correction to the direct output of the cascade code is a rather crude and incomplete way to simulate the binding energy of the nuclei. Furthermore, the simple experimental filter used in comparing intranuclear cascade predictions with experiment is not intended to simulate all biases. It does not include the double-track resolution or the track reconstruction inefficiencies, which can distort the experimental observables, especially for high-multiplicity events. For instance, the associated electronic dead time

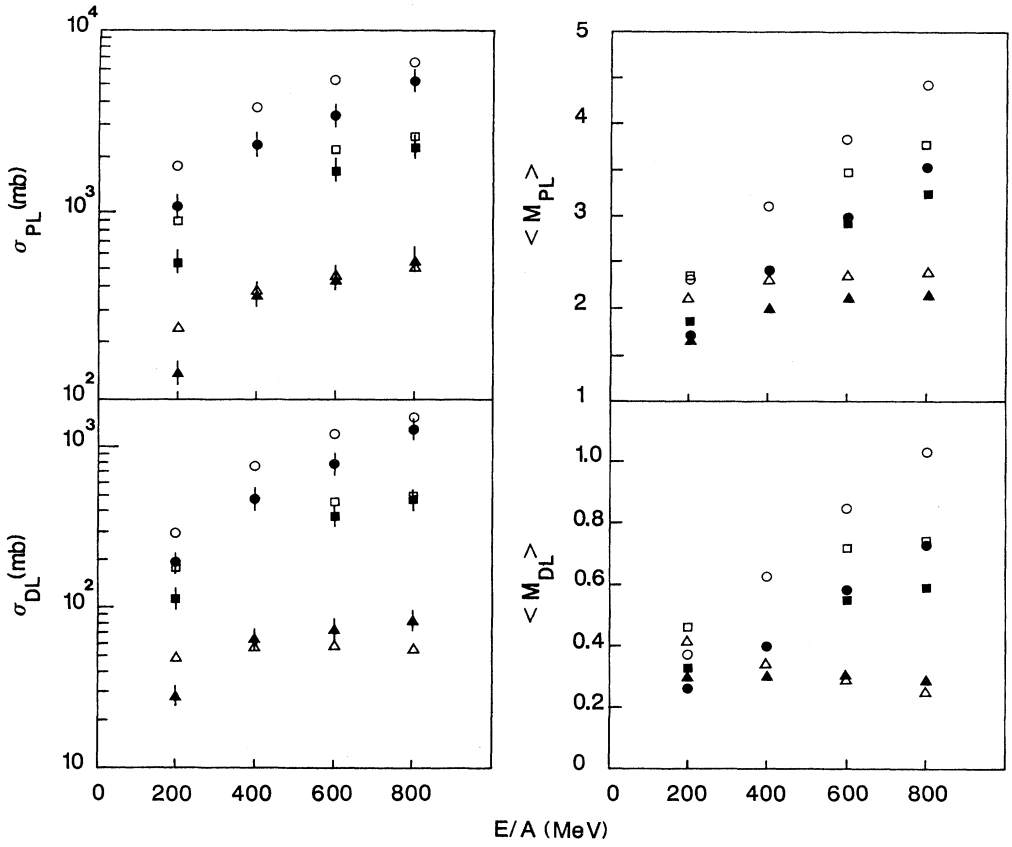

FIG. 15. Proton-like (top) and deuteron-like (bottom) cross sections (left), and mean proton-like (top) and deuteron-like (bottom) multiplicities (right) measured in DIOGENE vs the energy per nucleon of the α projectile. The experimental results (solid symbols) are compared to the cascade predictions (open symbols) for C (triangles), Cu (squares), and Pb (circles) targets. Experimental results are affected by a $\sim 15\%$ systematic error.

results in missed hits as the particle multiplicity increases, and consequently the double-track resolution deteriorates. Specifically, when the multiplicity of a charged particle emitted in the PDC acceptance is larger than ~ 10, some of them are not registered by the detector so that the measured multiplicity is lower than the real one.

Nevertheless, Fig. 16 shows that the experimental relation between the deuteron-like and proton-like multiplicities measured in DIOGENE are rather well reproduced by the cascade predictions. Only for $\alpha+C$ collisions does the experimental evolution of the mean deuteron-like multiplicity versus the mean proton-like multiplicity differ from the predicted one. But in the cascade the initial positions of the nucleons are randomly distributed within a sphere with uniform density. This simplification is certainly justified for heavy-target nuclei such as Pb and Cu, but not for the C nucleus, so that it simulates a

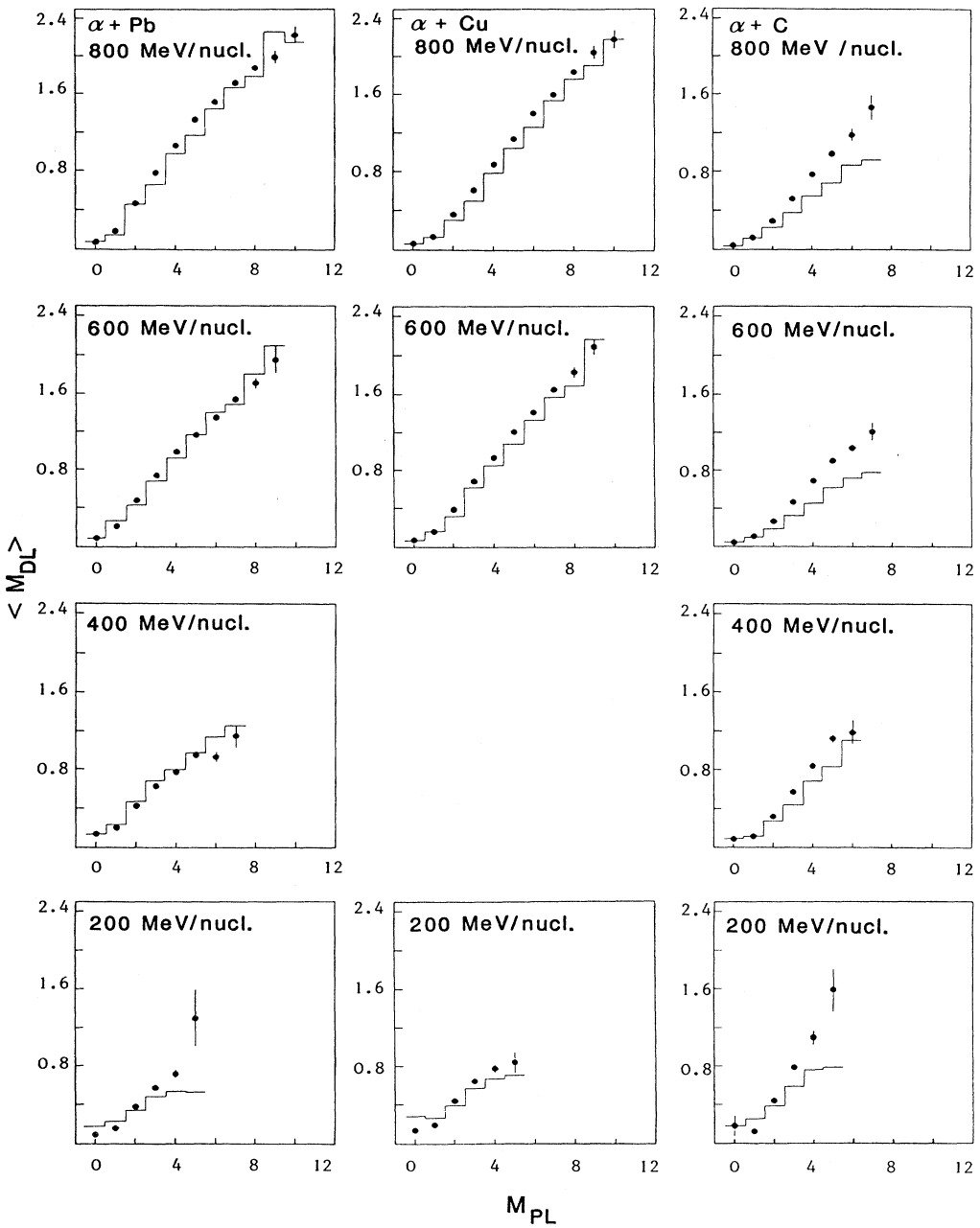

FIG. 16. Mean deuteron-like multiplicity measured in PDC deuteron acceptance versus the proton-like multiplicity measured in PDC proton acceptance for α-nucleus reactions at 800, 600, 400, and 200 MeV/nucleon (from top to bottom) on Pb (left), Cu (middle), and C (right) targets. The solid lines correspond to the cascade calculations.

spurious transparency of the C target to the incident α projectile.

Figures 17 and 18 show the experimental deuteron-like spectra compared to the cascade predicted ones. The main features of the dynamics are reproduced by the model, but the general agreement is better for the high incident bombarding energies (600 and 800 MeV/nucleon). At 400 and 200 MeV/nucleon incident energy, the model overpredicts the cross sections of deuteron-like particles emitted with low kinetic energy ($\sim$50–100 MeV) and large polar emission angle ($\theta \sim 50°$–$90°$).

V. CONCLUSION

We reported the deuteron production measurements in α-nucleus collision from 200 to 800 MeV/nucleon. They constitute the first part of a systematic study of the light-nuclear-fragment production in nucleus-nucleus collisions with the DIOGENE facility, ranging from this light projectile to larger incident nuclei (Ne and Ar). The relation between the inclusive parts of the observed proton and deuteron spectra indicates that the classic coalescence law holds reasonably well for such reactions with a light projectile nucleus. But this coalescence law remains a simplification since data from Ref. [44], as well as DIOGENE results, show that we have to examine momentum and angular dependences of the scaling constant in order to get a more clear insight onto the light-nuclear-fragment production in nucleus-nucleus collisions. The possibility of calculating theoretically the coalescence radius p_0 from the graph associated with the fusion between several nucleons [40] could be used in or-

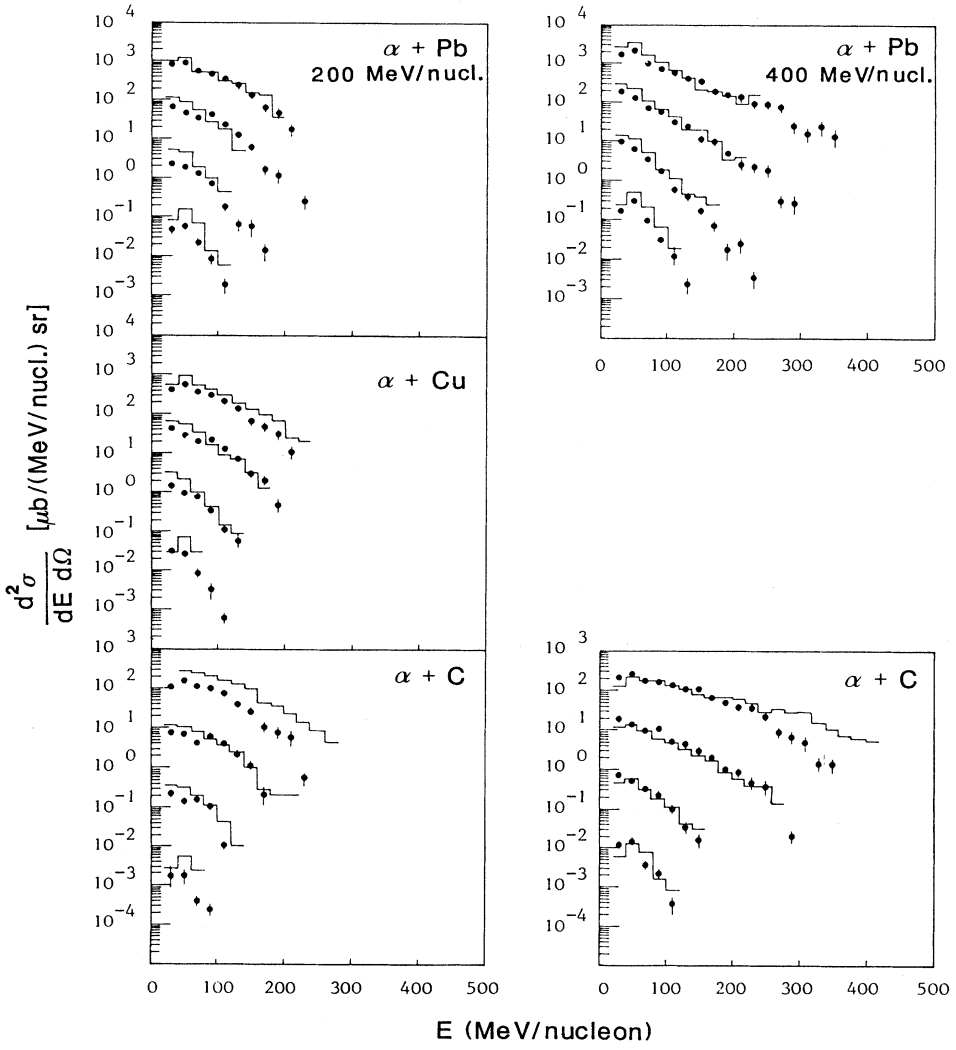

FIG. 17. Deuteron-like double-differential cross sections measured in 200- (left) and 400- (right) MeV/nucleon α+Pb, Cu, or C collisions. Kinetic energy per nucleon spectra at 30°, 50°, 70°, and 90° is shown for each reaction from top to bottom, multiplied by 1, 10^{-1}, 10^{-2}, and 10^{-3}, respectively. The experimental results are compared to the cascade predictions (solid lines). Only statistical errors bars are indicated, when larger than the symbols.

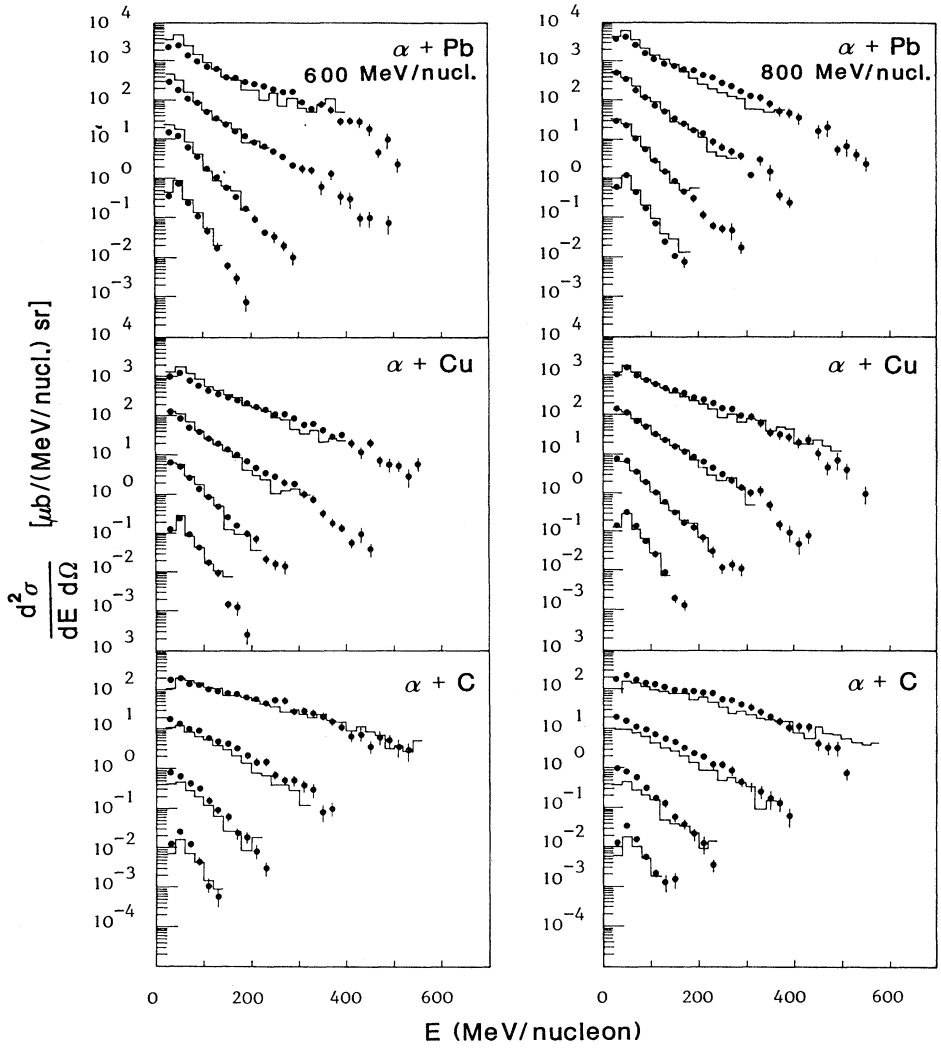

FIG. 18. Deuteron-like double-differential cross sections measured in 600- (left) and 800- (right) MeV/nucleon α+Pb, Cu, or C collisions. Kinetic energy per nucleon spectra at 30°, 50°, 70°, and 90° is shown for each reaction from top to bottom, multiplied by 1, 10^{-1}, 10^{-2}, and 10^{-3}, respectively. The experimental results are compared to the cascade predictions (solid lines). Only statistical errors bars are indicated, when larger than the symbols.

der to calculate the variation of the scaling constant. Nevertheless, the size of the interacting region can be evaluated from the measured scaling constants, and we obtain a radius of the order of 4 fm, depending of the target mass. These radii are consistent with the simple systematic parametrization by Nagamiya *et al.* [36], deduced from reactions with larger incident projectile nuclei.

The measured spectra of light particles have been used in order to test two rather different models of the reaction: a single-moving-source model with the assumption of a thermal equilibrium and a cascade model simulating the resolution of the Boltzmann equations of motion when the reaction is described as the succession of free nucleon-nucleon collisions. Comparisons between predicted and experimental spectra show that thermalization of the participant region could occur for low incident projectile energy (200 and 400 MeV/nucleon) and that the intranuclear model predictions agree better for 800- and 600-MeV/nucleon collisions.

*Present address: CRIP, H 1525 Budapest, Hungary.
†Present address: LNS, CEN Saclay, 91191 Gif-sur-Yvette Cedex, France.
‡Present address: NASA, Washington, DC 20546.

[1] S. T. Buttler and C. A. Pearson, Phys. Rev. **129**, 836 (1963).
[2] A. Schwarzchild and C. Zupancic, Phys. Rev. **129**, 854 (1963).

[3] H. H. Gutbrod, S. Sandoval, P. J. Johansen, A. M. Poskanzer, J. Gosset, W. G. Meyer, G. D. Westfall, and R. Stock, Phys. Rev. Lett. **37**, 667 (1976).
[4] J. Gosset, H. H. Gutbrod, W. G. Meyer, A. M. Poskanzer, S. Sandoval, R. Stock, and G. D. Westfall, Phys. Rev. C **16**, 629 (1977).
[5] M.-C. Lemaire, S. Nagamiya, S. Schnetzer, H. Steiner, and I. Tahinata, Phys. Lett. **85B**, 38 (1979).
[6] H. Sato and K. Yasaki, Phys. Lett. **98B**, 153 (1981).
[7] J. I. Kapusta, Phys. Rev. C **21**, 1301 (1980).
[8] B. J. Jennings, S. Das Gupta, and N. Mobed, Phys. Rev. C **25**, 278 (1982).
[9] R. Bond, P. J. Johansen, and S. E. Koonin, Phys. Lett. **71B**, 43 (1977).
[10] L. P. Csernai and J. I. Kapusta, Phys. Rep. **130**, 223 (1986).
[11] A. Mekjian, Phys. Rev. Lett. **38**, 640 (1977).
[12] A. Mekjian, Phys. Rev. C **17**, 1051 (1978).
[13] J. I. Kapusta, Phys. Rev. C **16**, 1493 (1977).
[14] J. Gosset, J. I. Kapusta, and G. D. Westfall, Phys. Rev. C **18**, 844 (1978).
[15] G. Bertsch and J. Cugnon, Phys. Rev. C **24**, 2514 (1981).
[16] V. D. Toneev and K. K. Gudima, Nucl. Phys. **A400**, 173c (1983).
[17] K. K. Gudima, V. D. Toneev, G. Köpke, and H. Shulz, Phys. Rev. C **32**, 1605 (1985).
[18] M. Gyulassy, K. Frankel, and E. A. Remler, Nucl. Phys. **A402**, 596 (1983).
[19] H. Stöcker, G. Buchwald, G. Graebner, P. Subramanian, J. A. Maruhn, W. Greiner, B. J. Jacak, and G. D. Westfall, Nucl. Phys. **A400**, 63c (1983).
[20] P. J. Siemens and J. I. Kapusta, Phys. Rev. Lett. **43**, 1486 (1979).
[21] H. J. Stöker, Nucl. Phys. **A418**, 587c (1984).
[22] K. G. R. Doss, H.-Å. Gustafsson, H. H. Gutbrod, B. Kolb, H. Löhner, B. Ludewigt, A. M. Poskanzer, T. Renner, H. Riedesel, H. G. Ritter, A. Warwick, and H. Wieman, Phys. Rev. C **32**, 116 (1985).
[23] D. Hahn and H. J. Stöcker, Nucl. Phys. **A452**, 723 (1986).
[24] L. P. Csernai, J. I. Kapusta, G. Fai, D. Hahn, J. Randrup, and H. Stöcker, Phys. Rev. C **35**, 1297 (1987).
[25] D. Hahn and H. J. Stöcker, Phys. Rev. C **37**, 1048 (1988).
[26] K. G. R. Doss, H.-Å. Gustafsson, H. H. Gutbrod, D. Hahn, K.-H. Kampert, B. Kolb, H. Löhner, A. M. Poskanzer, H. G. Ritter, H. R. Schmidt, and H. Stöcker, Phys. Rev. C **37**, 163 (1988).
[27] J. Kapusta and D. Strottman, Phys. Rev. C **23**, 1282 (1981).
[28] J. J. Molitoris, H. Stöcker, and B. L. Winer, Phys. Rev. C **36**, 220 (1987).
[29] J. Randrup, Nucl. Phys. **A314**, 429 (1979).
[30] J. W. Harris, G. Claesson, K. G. R. Doss, R. Ferguson, A. I. Gavron, H.-Å. Gustafsson, H. H. Gutbrod, B. V. Jacak, K. H. Kampert, B. Kolb, F. Lefebvres, A. M. Poskanzer, H. G. Ritter, H. R. Schmidt, L. Teitelbaum, M. Tincknell, S. Weiss, H. Wieman, and Wilhelmy, Nucl. Phys. **A471**, 241c (1987).
[31] H.-Å. Gustafsson, H. H. Gutbrod, J. Harris, B. V. Jacak, K. H. Kampert, B. Kolb, A. M. Poskanzer, H. G. Ritter, and H. R. Schmidt, Mod. Phys. Lett. A **3**, 1323 (1988).
[32] G. Peilert, Ph.D. thesis, University of Frankfurt, 1988.
[33] T. C. Awes, G. Poggi, C. K. Gelbke, B. B. Back, B. G. Glabola, H. Breuer, and V. E. Viola, Phys. Rev. C **24**, 89 (1981).
[34] T. C. Awes, S. Saini, G. Poggi, C. K. Gelbke, D. Cha, R. Legrain, and G. D. Westfall, Phys. Rev. C **25**, 2361 (1982).
[35] R. L. Auble, J. B. Ball, F. E. Bertrand, C. B. Fulmer, D. C. Hensley, I. Y. Lee, R. L. Robinson, P. H. Stelson, C. Y. Wong, D. L. Hendrie, H. D. Holmgren, and J. D. Silk, Phys. Rev. C **28**, 1552 (1983).
[36] S. Nagamiya, M.-C. Lemaire, E. Moeller, S. Schnetzer, G. Shapiro, H. Steiner, and I. Tanihata, Phys. Rev. C **24**, 971 (1981).
[37] B. V. Jacak, D. Fox, and G. D. Westfall, Phys. Rev. C **31**, 704 (1985).
[38] B. V. Jacak, G. D. Westfall, G. M. Crawley, D. Fox, C. K. Gelbke, L. H. Harwood, B. E. Hasselquist, W. G. Lynch, D. K. Scott, H. Stöcker, M. B. Tsang, G. Buchwald, and T. J. M. Symons, Phys. Rev. C **35**, 1751 (1987).
[39] S. Hayashi, Y. Miake, T. Nagae, S. Nagamiya, H. Hamagaki, O. Hashimoto, Y. Shida, I. Tahinata, K. Kimura, O. Yamakawa, T. Kobayashi, and X. X. Bai, Phys. Rev. C **38**, 1229 (1988).
[40] V. M. Kolybasov and Y. N. Sokolskikh, Phys. Lett. B **225**, 31 (1989).
[41] G. Montarou, Ph.D. thesis, University of Clermont II, 1988.
[42] J. P. Alard, J. P. Arnold, J. Augerat, R. Babinet, N. Bastid, F. Brochard, J. P. Costilhes, M. Crouau, N. De Marco, M. Drouet, P. Dupieux, H. Fanet, Z. Fodor, L. Fraysse, J. Girard, P. Gorodetzky, J. Gosset, C. Laspalles, M. C. Lemaire, D. L'Hôte, B. Lucas, G. Montarou, A. Papineau, M.-J. Parizet, J. Poitou, C. Racca, W. Schimmerling, J. C. Tamain, Y. Terrien, J. Valéro, and O. Valette, Nucl. Instrum. Methods A **261**, 379 (1987).
[43] J. Poitou, Nucl. Instrum. Methods **217**, 373 (1983).
[44] A. Sandoval, H. H. Gutbrod, W. G. Meyer, R. Stock, Ch. Luckner, A. M. Poskanzer, J. Gosset, J.-C. Jourdain, C. H. King, G. King, Nguyen Van Sen, G. D. Westfall, and K. L. Wolf, Phys. Rev. C **21**, 1321 (1980).
[45] S. Koonin, Phys. Lett. **70B**, 43 (1977).
[46] G. N. Agakishiyev, R. R. Mekhteev, V. Boldea, S. Ditza, J. Bartke, M. Kowalski, D. Armutliyski, J. J. Bogdanowicz, A. P. Cheplakov, L. A. Didenko, A. P. Gasparian, V. G. Grishin, I. A. Ivanovskaya, T. Kanarek, E. N. Kladnitskaya, D. K. Kopylova, V. B. Lyubimov, K. Millet, V. F. Nikitina, J. Pluta, M. I. Soloviev, R. Togoo, G. P. Toneeva, M. Chubarian, R. N. Bekmirzayev, U. D. Sherkulov, Z. V. Metreveli, and Z. Strugalski, Z. Phys. A **327**, 443 (1987).
[47] C. Cavata, M. Demoulins, J. Gosset, M.-C. Lemaire, D. L'Hôte, J. Poitou, and O. Valette, Phys. Rev. C **42**, 1760 (1990).
[48] C. Cugnon, Phys. Rev. C **22**, 1885 (1980).
[49] J. Cugnon, T. Mizutani, and J. Vandermeulen, Nucl. Phys. **A352**, 505 (1981).
[50] J. Cugnon and D. L'Hôte, Nucl. Phys. **A452**, 738 (1986).
[51] C. Racca, Ph.D. thesis, University of Strasbourg, 1987.